



Research article

The enhancement of dye filtration performance and antifouling properties in amino-functionalized bentonite/polyvinylidene fluoride mixed matrix membranes



Edi Pramono^{a,b}, Khairul Umam^{a,c}, Fuja Sagita^a, Ozi Adi Saputra^b, Rifki Alfiansyah^a, Rahmi Sri Setyawati Dewi^a, Grandprix T.M. Kadja^{a,d,e}, Mia Ledyastuti^a, Deana Wahyuningrum^f, Cynthia L. Radiman^{a,*}

^a Division of Inorganic and Physical Chemistry, Faculty of Mathematics and Natural Sciences, Institut Teknologi Bandung, Jalan Ganesha no. 10, Bandung, 40132, Indonesia

^b Chemistry Department, Faculty of Mathematics and Natural Sciences, Universitas Sebelas Maret, Jl. Ir. Sutami no. 36A, Surakarta, 57216, Indonesia

^c Textile Chemistry Division, Politeknik STTT Bandung, Jl. Jakarta no. 31, Bandung, 40272, Indonesia

^d Center for Catalysis and Reaction Engineering, Institut Teknologi Bandung, Jalan Ganesha no. 10, Bandung, 40132, Indonesia

^e Research Center for Nanosciences and Nanotechnology, Institut Teknologi Bandung, Jalan Ganesha no. 10, Bandung, 40132, Indonesia

^f Organic Chemistry Division, Faculty of Mathematics and Natural Sciences, Institut Teknologi Bandung, Jalan Ganesha no. 10, Bandung, 40132, Indonesia

ARTICLE INFO

Keywords:

PVDF

Silylation

Water treatment

Methylene blue

Acid yellow

ABSTRACT

Trade-off issue and membrane fouling remain two major issues in the utilization of membrane technology for the water treatment due to reduced membrane permeability and lifetime. In our study, we employed 3-aminopropyltriethoxysilane modified bentonite (BNTAPS) as an anti-fouling modifier to prepare polyvinylidene fluoride (PVDF)-based membranes via the phase inversion method. The effects of BNTAPS concentration on the physical, mechanical, morphological, and filtration performance of the hybrid membranes have been investigated. It was found that the addition of BNTAPS improved the hydrophilicity of the membrane revealed by the decreased water contact angle. Consequently, the pure water flux of PVDF membrane containing 0.5% BNTAPS (PVDF/BNTAPS0.5%) increased to $35.5 \text{ L m}^{-2} \text{ h}^{-1}$. Moreover, the PVDF/BNTAPS membrane showed a smaller pore diameter and porosity compared to pristine PVDF. The membrane performance evaluation was carried out using cationic and anionic dyes, i.e., methylene blue (MB) and acid yellow (AY17), respectively. Our study revealed that the rejection of each dye was slightly increased for the PVDF/BNTAPS0.5%. However, the flux recovery rate of the PVDF/BNTAPS membrane significantly improved, which directly prolonged the membrane lifetime.

1. Introduction

Providing clean water remains a fundamental problem in developing countries, including Indonesia. Contamination of clean water in Indonesia is dominantly caused by the poor industrial waste-disposal system, especially in the textile industry, which contains

* Corresponding author. Jl. Ganesha 10, Bandung, 40132, Indonesia.

E-mail addresses: cynthia@itb.ac.id, cynthia@chem.itb.ac.id (C.L. Radiman).

<https://doi.org/10.1016/j.heliyon.2023.e12823>

Received 2 August 2022; Received in revised form 31 December 2022; Accepted 3 January 2023

Available online 5 January 2023

2405-8440/© 2023 The Authors. Published by Elsevier Ltd. This is an open access article under the CC BY-NC-ND license (<http://creativecommons.org/licenses/by-nc-nd/4.0/>).

organic pollutants that are carcinogenic and difficult to degrade naturally [1,2]. Methods have been continuously developed to overcome this issue, for example, adsorption [3,4], photoelectrocatalytic degradation [5,6], and membrane technology [7-10]. Adsorption technology requires an immense quantity of adsorbents, which becomes a post-solid waste. Meanwhile, photoelectrocatalytic degradation consumes high energy for waste treatment. Compared to both methods, membrane technology offers a simple and green technology to cover up the shortcoming of those methods. A polymeric-based membrane water treatment technology is rapidly developed due to its advantages, including mild operating conditions, scalable, low energy consumption, and continuous processes [11].

Polyvinylidene fluoride (PVDF) is one of the promising organic polymers for membrane applications due to its good chemical resistance, high mechanical and physical properties, and excellent durability [12,13]. Therefore, this polymer is frequently used in microfiltration (MF), ultrafiltration (UF), and membrane distillation (MD) technology [14-18]. Nevertheless, the hydrophobicity of PVDF facilitates its interaction with organic molecules rendering fouling on the membrane surfaces, which reduces the membranes' lifetime [11,19]. Moreover, another crucial issue in the utilization of polymeric membrane is the trade-off between rejection and flux. It should be noted that the ideal membrane should have high rejection and fast flux simultaneously. However, this is difficult to be realized since a high rejection often sacrifice the flux and vice versa.

To overcome these issues, various modifications of PVDF membranes were performed for improving the hydrophilicity, membrane antifouling properties, and filtration performance. Several modifications had been reported, such as blending with polymers [19-21], combining with inorganic fillers to form mixed matrix membranes [22-25], and copolymerization of PVDF [26][27,28]. The addition of hydrophilic materials into PVDF membranes could improve the membrane performance and antifouling properties. Two types of components are widely used, i.e., polymer with polar end groups [23,24] and inorganic materials such as $Mg(OH)_2$ [21], Al_2O_3 [29], ZnO [20], CuO and $CaCO_3$ [30], Fe_2O_3 [31], TiO_2 [32], and ZrO [33,34]. The first type has a drawback in the mixing process, producing a less homogeneous membrane, while the second one shows advantages over polar polymers due to its easiness to fabricate, and capable of improving the membranes' physical properties and porosity. In addition, they do not possess porous structure that could function as the molecular sieve; thus, the filtration performance could not be significantly improved.

Another promising oxide material is bentonite (BNT) clay mineral with layered structures, found abundantly in Indonesia [35,36]. BNT is an aluminosilicate dominated by a montmorillonite (MMT) structure with negative charges on the frameworks. Furthermore, the layered structures exhibit the interlayer spaces that can swell when encounter water or other solvents; thus, enabling the sieving properties. The addition of BNT could improve the mechanical [37], and thermal properties of PVDF membranes [38], while the addition of polypyrrolidone-modified MMT produced a good performance toward Bovine Serum Albumin [39]. On the other hand, low concentration of Cloisite clay improved the PVDF membrane resistance toward surface abrasion [40]. Unfortunately, the exploration of BNT as PVDF membrane filler for water purification is still deemed limited.

In combining polymers with oxide materials, including BNT, one often encounters technical difficulty in which the ideal interaction between them is not ideal, either too strong or too weak. If they interact too strongly, the polymeric phase can undergo chain rigidification or densification that enhances the rejection but substantially reduces the flux. Alternatively, the interaction is too weak, leading to the formation voids that renders highly fast flux, but the rejection is sacrificed. Moreover, the addition of clay materials into hydrophobic polymer often produces agglomeration on the membrane surfaces due to surface tension difference between each component. Therefore, surface modification by an organosilane agent was introduced for modulating the hydrophobicity of the clay and facilitating the mixing process to make homogeneous membranes. The modification of clays by organosilanes, such as 3-aminopropyltriethoxysilane, (3-mercaptopropyl)trimethoxy silane and benzoyloxypropyltrimethoxy-silane have been successfully performed by previous researchers [41-44]. Shanmugharaj et al. reported that the highest amount of that silane compound grafted on the clay surface was obtained when water was used as the dispersion medium at 25 °C [45]. This modification changed not only the clay polarity but also the thermal properties [42].

To the best of our knowledge, the use of 3-aminopropyltrimethoxysilane (APS) in the synthesis of PVDF-BNTAPS membranes and their effects on the separation performance in the ultrafiltration process have not been studied yet. Therefore, in this work, we have performed a thorough investigation on the effects of BNTAPS on the hydrophilicity, physical properties, morphology, topography, and the performance of the PVDF-BNTAPS mixed matrix membranes for ultrafiltration of cationic and anionic dyes.

2. Experimental

2.1. Materials

Bentonite (BNT) was obtained from Bratachem Ltd. and sieved to pass 150 mesh. The silylating agent was 3-aminopropyl trimethoxysilane (APS) acquired from Sigma Aldrich. Polyvinylidene fluoride (PVDF) Solef® (MW = 573 kDa) was purchased from Solvay. The *N,N*-dimethylacetamide (DMAc), polyethyleneglycol (PEG, MW = 400) and polyethylene oxide (PEO, MW = 100,000 T-100) were available from Merck. Two dyes as models for examining the membrane performance were methylene blue (MB, MW = 319.85 g mol⁻¹, Merck) and acid yellow 17 (AY17, MW = 551.27 g mol⁻¹, Sigma Aldrich).

2.2. Synthesis of BNTAPS

Modification of BNT through the silylation method followed previous works procedure [36-38]. The BNT clay was dried for 24 h at 60 °C prior to the modification. About 5 g of BNT was added into a flask containing 250 mL of distilled water and stirred for 1 h. Afterward, 5 g of APS was slowly dropped, then reacted for 30 min and kept for another 30 min. The product was then filtered, washed

with distilled water, and dried overnight at 40 °C.

2.3. Preparation of PVDF/BNTAPS membrane

The PVDF/BNTAPS membrane was prepared through the phase inversion technique [46]. The BNTAPS was dispersed in DMAc by mechanical stirring for 1 h. Both PVDF and PEG were subsequently added into the dispersed BNTAPS and stirred for 24h at 60 °C. Next, the dope solution was sonically treated for 90 min at 60 °C and then casted on a glass plate using a tape with a thickness of 130 μm. This plate was directly dipped into a water bath containing distilled water at room temperature. The resulting membrane was washed repeatedly in flowing water and then stored in the glycerol solution. The composition of the dope solution followed a ratio of PVDF/PEG/BNTAPS/DMAc equal to 18/4/0–1/78–77 %w/w. Three membranes were prepared and coded as PVDF/BNTAPSx%, where the x values were 0, 0.5, and 1, respectively.

2.4. Characterization

The distinctive functional groups were characterized using ATR-FTIR (Alpha Bruker) to confirm the β fraction of each PVDF/BNTAPS composite. The sample was scanned for 48 times with a spectral resolution of 4 cm⁻¹. The polymorph of PVDF polymer was calculated using Equation (1).

$$F(\beta) (\%) = \left(\frac{A_{\beta}}{1.26A_{\alpha} + A_{\beta}} \right) \times 100 \quad (1)$$

where A_{β} and A_{α} are the absorbance at 840 cm⁻¹ and 763 cm⁻¹, respectively [40,46].

The hydrophobicity of membrane surfaces was analyzed by measuring their water contact angle using Mitutoyo sessile drop and recorded with Fujifilm Finefix S 13 MP camera and computed using software ImageJ. Water contact angle was recorded for three different position and reported value was the average number. Dynamic water contact angle was measured with same procedure for 45 min with a 5 min interval of measurement. The porosity of the membrane was characterized by the gravimetric method, and the largest pore size was measured using the bubble point method.

Membrane thermal property was analyzed by Hitachi DSC7000X. The membrane mechanical properties were characterized using Textechno Favigraph. Membranes with a dimension of 4 cm × 2 mm were measured at a speed of 50 mm/min in wet condition. Tensile strength, elongation and Young's modulus were computed and reported in this work.

The surface elements of membranes were analyzed using X-ray photoelectron Spectroscopy (XPS-ESCALAB VG Scientific) and energy dispersion X-ray (EDAX AMATEK Octane Pro). SEM JEOL JSM-6360LA observed the morphology of the membrane, while AFM Bruker recorded the topology of the membrane.

2.5. Analysis of membrane performance

The performance of membranes was determined by analyzing their water permeability and dyes selectivity using the dead-end microfiltration system at trans membrane pressure (TMP) 2 bar. In the first measurement, the pure flux membrane was determined by water feed. Afterward, two kinds of dyes, namely methylene blue (MB) and acid yellow-17 (AY-17) with concentration 1000 mg/L, were used as feed to determine the membrane rejection. Dyes structure were presented in Fig. 1a and b. Membrane water flux and rejection were calculated by Equations (2) and (3), respectively.

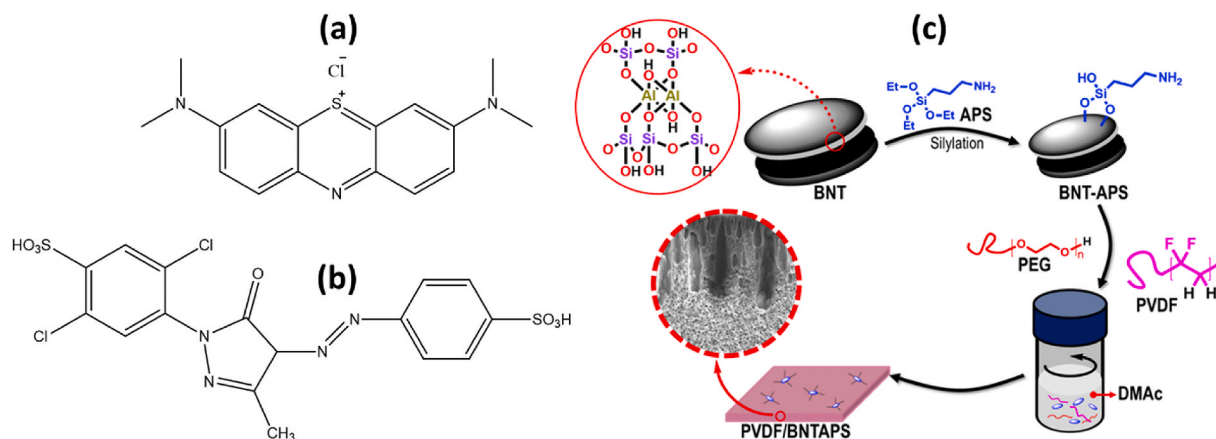


Fig. 1. The chemical structures of (a) Methylene Blue and (b) Acid Yellow 17. (c) Schematic synthesis of PVDF/BNTAPS membrane. (For interpretation of the references to colour in this figure legend, the reader is referred to the Web version of this article.)

$$J = \frac{v}{A \times t} \quad (2)$$

where J is water flux ($\text{L} \cdot \text{m}^{-2} \cdot \text{h}^{-1}$), v is volume of permeate (L), A is membrane area (m^2), and t is time (h).

$$\%R = \left(1 - \frac{C_p}{C_r}\right) \times 100 \quad (3)$$

in which R is rejection (%), C_p is concentration of permeate (g/L), and C_r is concentration of retentate (g/L). Antifouling properties of the membrane were determined by flux recovery ratio (FRR). Three sample models were used as feed, including PEO T-100, MB, and AY-17. In order to have the appropriate fluxes, three successive steps should be carried out, i.e., (i) measuring the pure water flux of the virgin membrane, (ii) changing the feed solution with either PEO T-100, methylene blue, or acid yellow and using these solutions as the feed for the filtration processes and washed afterward, (iii) remeasuring the pure water flux again. This process was carried out in two cycles, where each one gave the value of FRR-1 and FRR-2, respectively. The FRR of the membrane was calculated according to Equation (4)

$$\text{FRR} = \frac{J_n}{J_0} \times 100\% \quad (4)$$

where J_0 is first step pure water flux, and J_n is the pure water flux of cleaned membrane after n cycle.

3. Results and discussion

3.1. Structural analysis of the PVDF/BNTAPS membranes

The PVDF/BNTAPS membranes have been successfully prepared through the phase inversion method by incorporating a small amount of BNTAPS (maximum 1 %wt), as illustrated in Fig. 1c. BNT as a clay mineral was used as an inorganic filler modified with APS to introduce amines functional groups, and later called BNTAPS. Further, the BNTAPS was introduced into the polymer solution, homogenized, casted and kept in glycerin solution for future use. As a result, a homogeneous membrane appearance was clearly observed, indicating a small amount of BNTAPS is compatible with the PVDF polymer.

Surface elemental compositions of PVDF/BNTAPS membrane were analyzed by XPS and EDAX techniques. Fig. 2a depicts the XPS

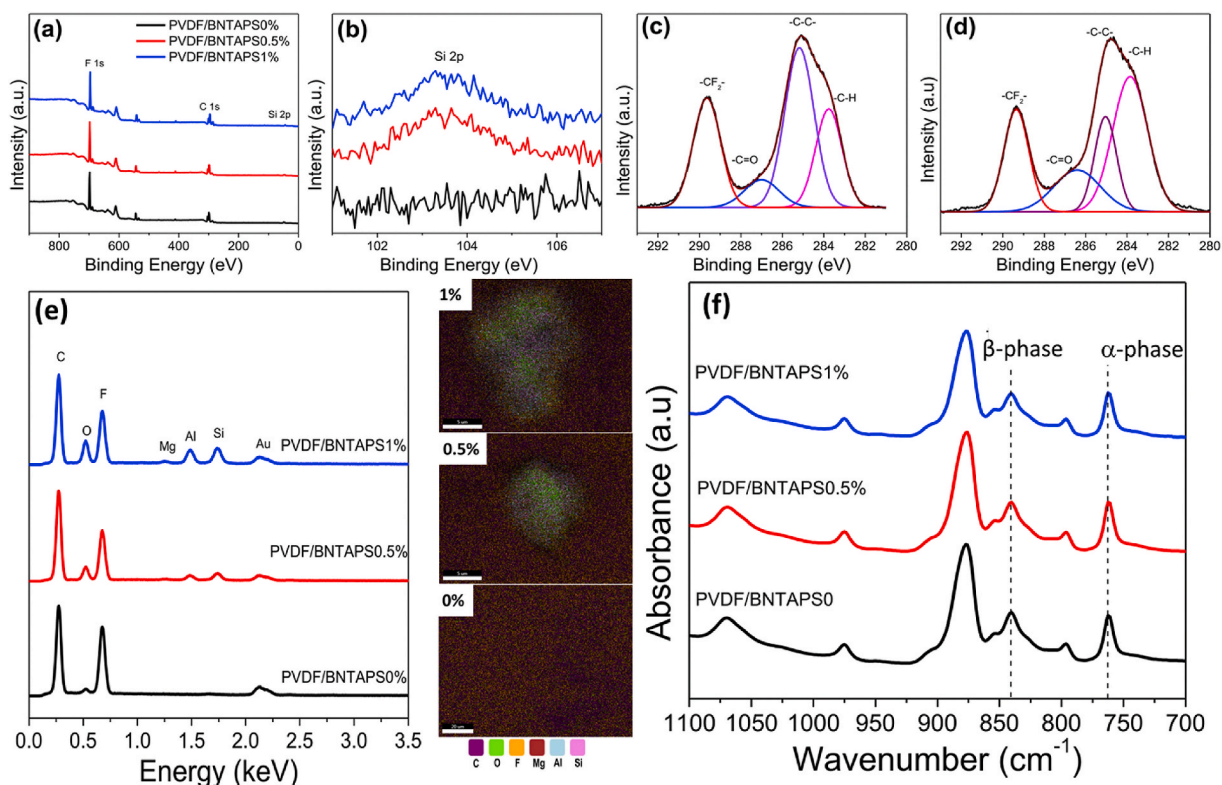


Fig. 2. (a) XPS and (b) Si 2p core-level XPS spectra of PVDF/BNTAPS hybrid membranes; C 1s core-level XPS spectra of (c) PVDF/BNTAPS0% and (d) PVDF/BNTAPS0.5%. (e) EDS spectra and the corresponding elemental mapping, and (f) ATR-FTIR spectra of PVDF/BNTAPS membranes.

full spectra of PVDF and PVDF/BNTAPS membranes, revealing the C 1s and F 1s typical core peaks of PVDF appear at around 300 eV and 700 eV, respectively. In addition, a typical Si 2p peak is observed at 103.6 eV in PVDF/BNTAPS XPS spectra, which is not found in pristine PVDF XPS spectra. The Si 2p core-level spectrum shows that the peak intensifies by increasing BNTAPS concentration, as depicted in Fig. 2b. The analysis of the C element on the membranes was carried out by scanning the sample between 280 eV and 293 eV. Fig. 2c shows the deconvolution of C 1s core-level spectra of PVDF, indicating $-\text{CF}_2$, C–O, C–C, and C–H typical peaks found at 289.5, 287, 285, and 283.5 eV, respectively [47]. These peaks are also found in the PVDF/BNTAPS C 1s core-level spectra, but both C–O and $-\text{CF}_2$ peaks slightly shift to 286.5 and 289 eV, respectively, caused by PVDF–BNTAPS interaction. Moreover, the peak intensity of $-\text{CH}_2$ is higher than C–C, as depicted in Fig. 2d. This is due to the interaction between BNTAPS and PVDF involving hydrogen atoms of PVDF, as reported by Zhang et al. [38].

The elemental composition of PVDF/BNTAPS membranes was characterized by SEM-EDAX (Fig. 2e). The pristine PVDF membrane comprises three main elements, i.e., C, O and F. New peaks associated with Al and Si elements that originate from the clay structure are observed in the PVDF/BNTAPS EDAX spectra. Moreover, the O element peak intensity is enhanced along with the increasing BNTAPS concentrations. The presence of BNTAPS on the membrane matrix can be detected by the appearance of Si and Al elements. The content of elements was found close to the total amount of BNTAPS added into the dope solution. Moreover, Fig. 2e also reveals the elemental mapping generated from EDS analysis of some major elements of PVDF and PVDF/BNTAPS membranes. The Si and Al elements can be distinguished on the surface of the membranes, except for pristine PVDF membranes. Furthermore, the effect of BNTAPS addition toward the polymorph structure of PVDF is analyzed using ATR-FTIR, as shown in Fig. 2f. The data indicates that the membranes are composed of α - and β -phases of PVDF confirmed by the presence of typical peaks of both α - and β -phases appeared at 760 cm^{-1} and 840 cm^{-1} , respectively. The addition of BNTAPS slightly reduces the β -phase of PVDF. Thus, the surface modification of BNT by the organosilane agent could decrease its polarity.

3.2. Physico-mechanical and surface properties of the PVDF/BNTAPS membranes

Thermal properties of the membranes were analyzed using the differential scanning calorimetry (DSC). The DSC curves and the melting temperatures (T_m) of PVDF/BNTAPS0% and PVDF/BNTAPS0.5%, as depicted in Fig. 3a. The thermal properties of both materials appear to be similar in which the PVDF/BNTAPS0% and PVDF/BNTAPS0.5% exhibit the T_m of $161.16\text{ }^\circ\text{C}$ and $160.18\text{ }^\circ\text{C}$, respectively. This indicates that the BNTAPS could well interact with the PVDF matrices and did not significantly alter the PVDF structure. Moreover, Fig. 3b shows the mechanical properties of the PVDF and PVDF/BNTAPS mixed matrix membranes. The tensile strength of the membrane is slightly affected by the presence of BNTAPS. The Young modulus of the membranes declines at 0.5% and 1% w/w of BNTAPS. The presence of silane groups on BNTAPS facilitates the clay interaction with PVDF polymer, making the polymer segment easy to penetrate the BNT structure. The mechanical tests confirmed that the mixed matrix membranes become stronger to hold the force given to their transition area. However, a high concentration of BNTAPS leads to a drop in the membrane elasticity, as shown by the increase of membrane Young modulus.

Table 1 provides the comparisons of physical parameters, including water contact angle, pore-radius, porosity, membrane thickness water flux and molecular weight cut-off (MWCO) of each PVDF/BNTAPS membrane. Generally, the addition of BNTAPS influences the properties of the resulting membranes. For example, the presence of polar BNTAPS transforms the membrane to be more hydrophilic, proven by the decrease of water contact angle. It also induces the decrease of pore radius and porosity of the membrane. Consequently, the MWCO of the membrane shifts from high to low molecular weight molecules, indicating the improved selectivity of the membranes. Moreover, the addition of BNTAPS reduced the membrane thickness. In general, it is known that the thicker the membrane, the lower the water permeation capacity. This study obtained the lower pure water flux and the MWCO value. Therefore, it can be concluded that the pore property is more dominant in influencing the filtration process.

The surface membrane hydrophilicity was analyzed by dynamic contact angle and presented in Fig. 3c. The initial water contact angle of pristine PVDF membrane is 71.53° , which decreases along with the addition of BNTAPS, indicating the improvement of

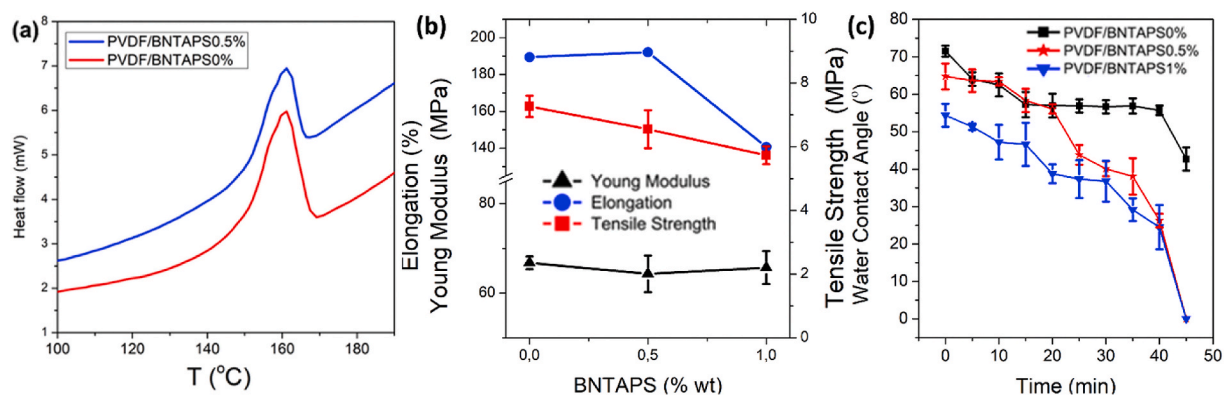


Fig. 3. (a) DSC curves, (b) mechanical properties, and (c) dynamic water contact angle of PVDF/BNTAPS membranes. The deviations in (b) and (c) are based on three measurements.

Table 1

Physical parameters of pristine and hybrid membranes at various composition of BNTAPS. The deviations are based on three measurements.

Parameters	BNTAPS (% wt)		
	0	0.5	1
Water contact angle ($^{\circ}$)	71.53 \pm 1.50	64.76 \pm 3.50	54.36 \pm 3.06
Pore diameter ($\times 10^{-1}\mu\text{m}$)	8.90 \pm 0.08	5.84 \pm 0.02	4.65 \pm 0.02
Porosity (%)	69.36 \pm 2.19	62.97 \pm 3.63	54.83 \pm 3.24
Membrane thickness (μm)	93.60 \pm 0.89	84.20 \pm 0.84	85.60 \pm 0.89
Pure water flux ($\text{L}\cdot\text{m}^{-2}\cdot\text{h}^{-1}$)	30.83 \pm 1.04	35.5 \pm 2.08	16.00 \pm 3.61
MWCO at 90% rejection (kDa)	97.57	88.79	86.28

hydrophilicity. The water contact angle of pristine PVDF is not significantly altered over the dynamic measurement of water contact time. On the contrary, the water contact angles of PVDF/BNTAPS0.5% and PVDF/BNTAPS1% dramatically alter after being contacted for 20 min and drop to below 20° at 45 min. Accordingly, the addition of 0.5% and 1% BNTAPS significantly improves the hydrophilicity of the membranes.

The addition of BNTAPS on the membranes produces low membrane porosity. The membrane pore formation is influenced by the solvent and coagulant interchange rate, and the presence of PEG as porogen. PEG generates the pore formation on the membrane surfaces and cross-section. The presence of BNTAPS decelerates the exchange rate of solvent and coagulant. Additionally, BNTAPS also reduced the rate release of PEG, causing small membrane pores' formation.

The use of BNTAPS produces membranes with smaller surface pore diameters compared to pristine PVDF membranes. The non-polar organosilane agents enhances the interaction between the BNT and PVDF due to the minimized repulsion between polar groups of BNT and non-polar PVDF, forming a more compact pore structure. As a result, the largest pore diameter is found to be 0.46 μm for PVDF/BNTAPS1% membrane, which is smaller than that of the pristine PVDF membrane (0.84 μm). Based on their pore diameter, both pristine PVDF and mixed matrix membranes are categorized as microfiltration membranes [48]. The pure water flux increases by adding 0.5% BNTAPS but decreases with 1% w/w of BNTAPS. The decrease in water flux of the mixed matrix membranes is in good agreement with the decreasing membrane porosity and pore size, showing the hydrophilic membrane surfaces improve the water-surface interactions.

3.3. The PVDF/BNTAPS membrane performances

Fig. 4a shows the flux and rejection of PVDF/BNTAPS membranes toward cationic and anionic dyes, like methylene blue (MB) and acid yellow (AY17). The presence of 0.5% w/w BNTAPS improves the flux of MB permeate, but it decreases by 1% w/w of BNTAPS. Meanwhile, the flux of AY17 permeates increases with the increase of BNTAPS concentration. Moreover, the presence of BNTAPS also shows an improvement of membrane rejection toward both dyes. However, the PVDF/BNTAPS1% has lower rejection compared to other membranes.

Mixed matrix membranes can retain most MB dyes shown by the high rejection values, more than 90%, but much less for AY17 rejecting around 70%. A higher rejection value of MB is achieved by PVDF/BNTAPS1%, about 97%. Meanwhile, it is PVDF/BNTAPS0.75% having the highest AY17 rejection of 79%. It is known that the filtration process is influenced by surface properties, pore size and membrane porosity. The addition of BNTAPS produces a compact mixed matrix membrane and hydrophilic surface nature. Consequently, the membrane surface can retain the dye and increase its rejection value. The highly hydrophilic character and the presence of BNTAPS on the membrane surfaces will force the MB interaction on the membrane surfaces, which keeps the MB longer on the membrane surfaces. Interaction between dye molecules is frequently forming larger molecules. Although MB has a lower

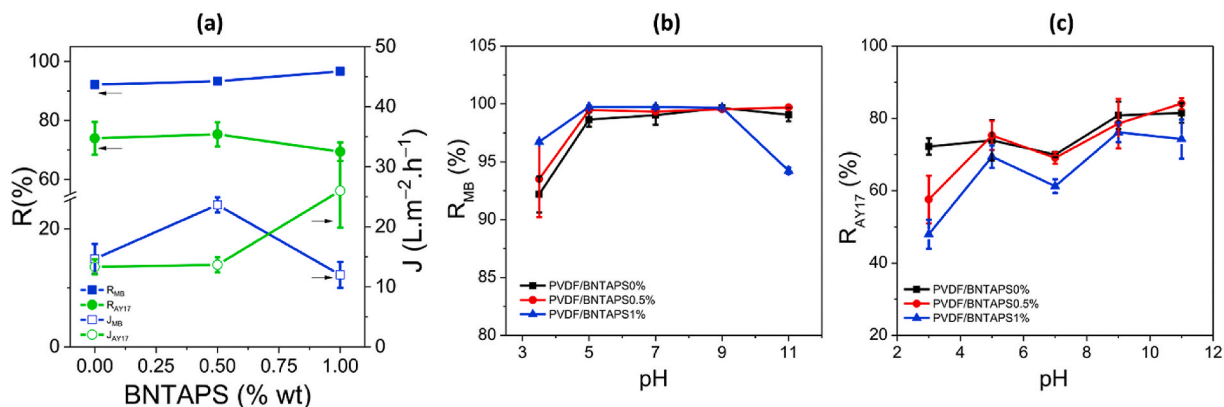


Fig. 4. (a) Rejection and water flux of hybrid membrane, and effect of pH toward (b) MB and (c) AY17 rejection of PVDF and PVDF/BNTAPS membranes. The deviations are based on three measurements.

molecular weight compared to AY17, the membrane shows better filtration performance against it. Golz et al. reported that MB could form dimer structures and combine up to five molecules at high concentrations, directly increasing the MB molecule dimension [49]. The aggregation phenomenon of MB could contribute to low MB permeation passing through the membrane. It should also be emphasized that the addition of bentonite clay, which tends to be negatively charged, impacts the higher interaction of cationic dyes on the membrane surface. MB is a cationic dye that will interact more strongly on the surface of the membrane, leading to a higher rejection.

In general, pH influences the membrane performance due to the charges of dyes or the changing of dyes structure depending on pH [50]. As shown in Fig. 4b, the MB rejection values are elevated by the increasing pH of the feed solution. The rejection value of PVDF/BNTAPS1% mixed matrix membrane is higher than that of pristine PVDF and PVDF/BNTAPS0.5% membranes but declines at pH 11 while the other two are relatively constant. Similarly, as depicted in Fig. 4c, the AY17 rejection values increase with the increase of feed solution pH. Since the presence of BNTAPS also contributes a negative charge to the PVDF membrane surface, the resulting membrane has better performance in basic conditions. However, the filtration of AY17 is influenced by the rate of water molecules permeated on the membrane pores due to the same charges between AY17 and the membrane surface. Rejection of AY17 from PVDF/BNTAPS mixed matrix membranes showed a slight improvement, but still below 90%, and it was lower than the pristine PVDF membranes. This is probably due to the dimension of AY17 molecules being relatively the same or lower than the membrane pore diameter. The increase of the membrane surfaces' negative charge with the presence of BNTAPS causes the AY17 to escape from the membrane surfaces easily. Increasing the pH value made the membrane surfaces more negative, improving their interaction with water and speeding up the water permeation rate. Table 2 shows the comparison of dye rejection ability between various PVDF-based membranes. The modified PVDF membrane either by oxide, surfactant or organic polymer reveals a good dye rejection ability with more than 90%. Our material (PVDF/BNTAPS0.5%) indicate a potency as membrane filtration for treating wastewater containing dye with dye rejection ability of more than 90%.

The anti-fouling properties of the membrane were analyzed by measuring the water flux recovery ratio (FRR). Fig. 5a and d presents the membrane permeate profile and FRR for filtration of non-ionic PEO T-100, respectively. The mixed matrix membrane shows better anti-fouling than the pristine PVDF. After washing, the mixed matrix membranes have higher water flux compared to those of pristine PVDF membranes, as shown by higher FRR-1 and FRR-2. It indicates that the PEO T-100 molecules were relatively easy to detach from the mixed matrix membrane surface during the washing process. Fig. 5(b) and (e) show the permeate profile and FRR values of the MB filtration. In the case of the PEO T-100, the PVDF/BNTAPS mixed matrix membranes show a higher flux value after the washing process. PVDF/BNTAPS0.5% membranes achieve the higher FRR-1 and FRR-2 values of the MB filtration, but contrary phenomena are observed for the PVDF/BNTAPS1%.

The FRR value on the filtration of AY17 is higher than MB filtration (Fig. 5c and (f)), reaching an average value of 60% for AY17 and 51% for MB. The easiness of flocculants recovery from the membrane surfaces could be affected by the interaction strength and the roughness of the membrane surface. The BNTAPS contributes the negative charges, which ionically interact with the cationic MB dye, but repulse the anionic AY17. Consequently, the MB molecules were bound more tightly to the membrane surfaces and more difficult to be detached during the washing process. The roughness of membrane surfaces also influences the release of dye molecules during the washing process—higher roughness results in a greater possibility of fouling phenomena.

3.4. Morphological and topological studies of the PVDF/BNTAPS membranes

The morphology of PVDF/BNTAPS membrane surfaces and cross-sections is presented in Fig. 6a-f. The pristine PVDF and mixed matrix membrane surfaces have similar morphology. Fig. 6c-d reveals the cross-section of PVDF/BNTAPS, indicating the membrane's asymmetric structure, which consists of a thin layer on the surface, finger-like macropores, and sponge-like micropores. A similar

Table 2
Comparison of the PVDF-based membranes toward the capability in dye rejection.

Materials	General properties	Dyes	Rejection	Ref.
PVDF/Fe ₃ O ₄ -HNTs	Water contact angle = 60.7° Flux = 26.7 L m ⁻² h ⁻¹	Methylene blue	84.7% (Dead-end; Pressure 3 bar)	[51]
PVDF/Brij-58	Water contact angle = 46° Pure water flux = 31.2 ± 2 L m ⁻² h ⁻¹ MWCO = 570 ± 20 Da	RR141	90 ± 1.4% (6 bar, continuous flow)	[52]
PVDF/Chitosan/CNT	Pure water flux = 85.25 L m ⁻² h ⁻¹ Water contact angle = 70.4°	CV, RB, SY, MB, MeB, CR	>90% (dead-end, Pressure of 0.2 MPa)	[53]
PVDF/MWCNT	Pure water flux = 138 L m ⁻² h ⁻¹ Porosity = 86.2 ± 2.9% Mean pore size = 7.23 ± 1.1 nm, Qater contact angle = 56.9 ± 4.3°	Reactive Green 19	97.3% (dead-end, 4 bar at first 10 min than reduce to 3 bar afterward)	[54]
PVDF/GO/Ni	Water flux = 38.39 L m ⁻² h ⁻¹ bar ⁻¹ water contact angle = 11.9°.	Congo Red	98.02% (dead-end, 0.1 MPa)	[55]
PVDF/Fe ₃ O ₄ /MIP	Water flux = 42.5 L m ⁻² h ⁻¹ Water contact angle of 58.72°	Rhodamine B	95.8% (semi continuous-flow, 3 bar of pressure)	[56]
PVDF/BNTAPS0.5	Pure water flux 35.5 L.m ⁻² h ⁻¹ , water contact angle 64.76 ± 3.5°, porosity 62.97 ± 3.63%,	MB	~90% (dead-end, pressure of 2 bar)	This work

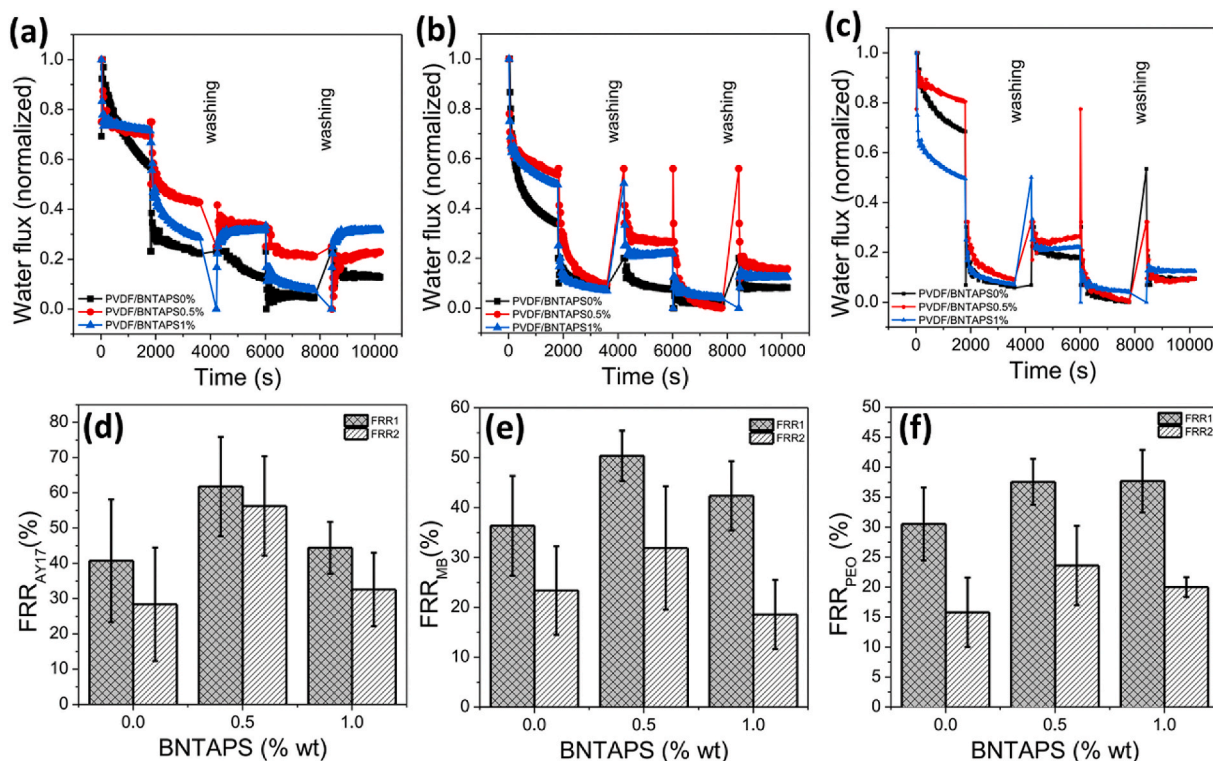


Fig. 5. (a–c) Flux profile over measuring time and (d–f) effect of BNTAPS toward FRR of (a,d) PEO-T-100, (b,e) MB, and (c,f) AY17. The deviations in (d–f) are based on three measurements.

morphological structure was also reported by previous work utilizing clay minerals to modify PVDF [40]. The finger-like macropore was formed during phase inversion caused by fast solvent-coagulant exchange. A penetration rate of non-solvent is influenced by the viscosity of the polymer solution, in which the penetration rate will be slower for the high viscous solution. This situation leads to a slow formation of the membrane layer.

The macropore is also affected by the release of PEG molecules from the system-enriched polymer into the coagulant component. The presence of BNTAPS induces the shortening of the macropore channel due to the slow rate of solvent released into the coagulant system. The clay minerals could initially adsorb the solvent into its structure, making a slow exchange rate of solvent and non-solvent. The membrane surface topography measured by AFM is presented in Fig. 6g-l. A two-dimension (2D) image reveals no significant differences between the pristine PVDF and PVDF/BNTAPS membranes. Moreover, the three-dimension (3D) topography image indicates the membrane surfaces constructed by hills and valleys. The addition of BNTAPS produces a broad valley pattern, while hills dominate the pristine PVDF membrane.

Quantitatively, as shown in Table 3, the roughness of the pristine PVDF membranes is higher than the mixed matrix membranes. So, the addition of BNTAPS results in broader valleys and fewer hills, which decrease the membrane roughness. The formation of hills and valleys occurred during the phase inversion. The hydrophilic parts of the dope solution, namely the PEG, facilitate the interaction with the coagulant. On the other hand, the hydrophobic parts interact with PVDF during the liquid-liquid demixing process. Therefore, the formation of hills and valleys is homogeneous. The presence of oxide in the solution disturbs the release of PEG and the solvent, decreasing the membranes' surface roughness, as indicated in Table 3. Thus, the lower surface roughness results in a lower membrane contact angle, which leads to a better antifouling membrane.

4. Conclusions

The PVDF/BNTAPS membrane was successfully prepared through the phase-inversion method. The surface analysis by XPS and EDS revealed that the BNTAPS was also deposited on the membrane surfaces. The presence of BNTAPS on the PVDF membrane significantly influenced the properties and performance of the membrane. Furthermore, the water contact angle of the membrane was decreased with the increase of BNTAPS concentration. In addition, the pore diameter and porosity of the membrane also decreased. However, the pure water flux was only improved for PVDF/BNTAPS0.5. The PVDF/BNTAPS0.5 membrane showed high rejection over MB and AY17 of ~90% and ~70%, respectively. In addition, the water fluxes in both MB and AY17 filtrations over PVDF/BNTAPS0.5 were enhanced as compared to the pristine PVDF. The filtration performance's enhancement could be related to the suitable interaction between the PVDF matrix and the amine-functionalized bentonite. Ultimately, BNTAPS as an anti-fouling agent positively

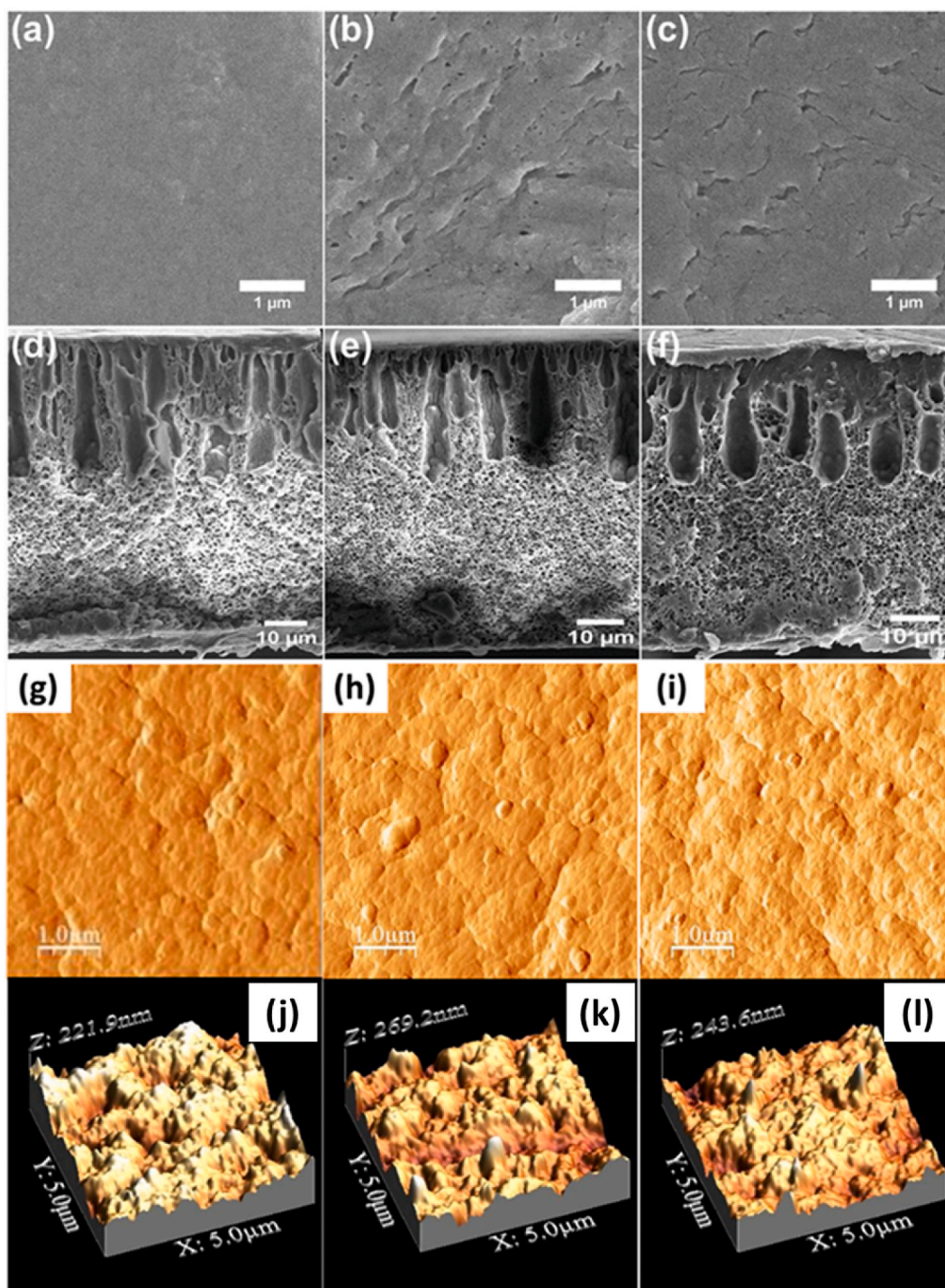


Fig. 6. (a–c) Surface, (d–f) cross-section SEM images, and (g–i) AFM images and (j–l) the corresponding contour mapping of PVDF membrane surfaces and cross-section with various concentration of BNTAPS: (a,d,g, j) 0%, (b,e,h, k) 0.5% and (c,f,i, l) 1% w/w.

Table 3

The surface roughness of PVDF and PVDF/BNTAPS membranes. The deviations are based on three measurements.

Membranes	R _q (nm)	R _a (nm)
PVDF/BNTAPS0%	27.42 ± 0.20	22.07 ± 0.20
PVDF/BNTAPS0.5%	9.88 ± 0.82	7.48 ± 0.45
PVDF/BNTAPS1%	8.38 ± 0.49	6.38 ± 0.47

impacted the improvement of FRR value compared to PVDF pristine membrane. Therefore, improvement of selectivity, anti-fouling performance, and low-cost raw materials of PVDF/BNTAPS provide potential application in wastewater treatment.

Author contribution statement

Edi Pramono: Performed the experiments, analyzed and interpreted the data, wrote the paper. Khairul Umam: Performed the experiments, wrote the paper. Fuja Sagita: Performed the experiments, wrote the paper. Ozi Adi Saputra: Performed the experiments. Rifki Alfiansyah: Performed the experiments. Rahmi Sri Setyawati Dewi: Performed the experiments. Grandprix T.M. Kadja: Conceived and designed the experiments, contributed reagents, materials, analysis tools or data, wrote the paper. Mia Ledyastuti: Conceived and designed the experiments, wrote the paper. Deana Wahyuningrum: Conceived and designed the experiments, Wrote the paper. Cynthia L. Radiman: Conceived and designed the experiments, contributed reagents, materials, analysis tools or data, wrote the paper.

Funding statement

This work was supported by the Ministry of Education, Culture, Research and Technology (Kemdikbudristek) of the Republic of Indonesia under the contract of World Class Research (WCR) Program 2021 (079/E4.1/AK.04.PT/2021).

References

- [1] E. Routoula, S.V. Patwardhan, Degradation of anthraquinone dyes from effluents: a review focusing on enzymatic dye degradation with industrial potential, *Environ. Sci. Technol.* 54 (2020) 647–664, <https://doi.org/10.1021/acs.est.9b03737>.
- [2] O.A. Saputra, M. Nauqinida, Kurnia, S. Pujiasih, T. Kusumaningsih, E. Pramono, Improvement of anionic and cationic dyes removal in aqueous solution by Indonesian agro-waste oil palm empty fruit bunches through silylation approach, *Groundw Sustain. Dev.* 13 (2021), 100570, <https://doi.org/10.1016/j.gsd.2021.100570>.
- [3] V. Meshko, L. Markovska, M. Mincheva, A.E. Rodrigues, Adsorption of basic dyes on granular activated carbon and natural zeolite, *Water Res.* 35 (2001) 3357–3366, [https://doi.org/10.1016/S0043-1354\(01\)00056-2](https://doi.org/10.1016/S0043-1354(01)00056-2).
- [4] O.A. Saputra, Kurnia, S. Pujiasih, V.N. Rizki, B. Nurhayati, E. Pramono, et al., Silylated-montmorillonite as co-adsorbent of chitosan composites for methylene blue dye removal in aqueous solution, *Commun. Sci. Technol.* 5 (2020) 45–52, <https://doi.org/10.21924/cst.5.1.2020.182>.
- [5] S. Wahyuningsih, C. Purnawan, T.E. Saraswati, E. Pramono, A.H. Ramelan, S. Pramono, et al., Visible light photoelectrocatalytic degradation of rhodamine B using Ti/TiO₂-NiO photoanode, *J. Environ. Protect.* 5 (2014) 1630–1640, <https://doi.org/10.4236/jep.2014.517154>.
- [6] S. Aflaki, M. Farhadian, A.R. Solaimany Nazar, S. Tangestaninejad, N. Davari, Investigation of copper plates as anode and TiO₂/glycine/ZnFe₂O₄ stabilized on graphite as cathode for textile dyes degradation from aqueous solution under visible light, *J. Appl. Electrochem.* (2021), <https://doi.org/10.1007/s10800-021-01580-y>.
- [7] P. Zhao, R. Li, W. Wu, J. Wang, J. Liu, Y. Zhang, In-situ growth of polyvinylpyrrolidone modified Zr-MOFs thin-film nanocomposite (TFN) for efficient dyes removal, *Compos. B Eng.* 176 (2019), 107208, <https://doi.org/10.1016/j.compositesb.2019.107208>.
- [8] S. Zhou, J. Gao, J. Zhu, D. Peng, Y. Zhang, Y. Zhang, Self-cleaning, antibacterial mixed matrix membranes enabled by photocatalyst Ti-MOFs for efficient dye removal, *J. Membr. Sci.* 610 (2020), 118219, <https://doi.org/10.1016/j.memsci.2020.118219>.
- [9] V. Vatanpour, S.S. Mousavi Khadem, A. Dehqan, M.A. Al-Naqshabandi, M.R. Ganjali, S. Sadegh Hassani, et al., Efficient removal of dyes and proteins by nitrogen-doped porous graphene blended polyethersulfone nanocomposite membranes, *Chemosphere* 263 (2021), 127892, <https://doi.org/10.1016/j.chemosphere.2020.127892>.
- [10] A. Wibowo, M.A. Marsudi, E. Pramono, J. Belva, A.W.Y.P. Parmita, A. Patah, et al., Recent improvement strategies on metal-organic frameworks as adsorbent, catalyst, and membrane for wastewater treatment, *Molecules* 26 (2021) 1–32, <https://doi.org/10.3390/molecules26175261>.
- [11] Y. Li, Q. Qi, S. Shan, Z. Yao, F. Liu, B. Zhu, The stabilization of ultrafiltration membrane blended with randomly structured amphiphilic copolymer: micropollutants adsorption properties in filtration processes, *J. Colloid Interface Sci.* 613 (2022) 234–243, <https://doi.org/10.1016/j.jcis.2022.01.055>.
- [12] J. Zhu, S. Zhou, M. Li, A. Xue, Y. Zhao, W. Peng, et al., PVDF mixed matrix ultrafiltration membrane incorporated with deformed rebar-like Fe₃O₄-polyglycorkite nanocomposites to enhance strength and antifouling properties, *J. Membr. Sci.* 612 (2020), 118467, <https://doi.org/10.1016/j.memsci.2020.118467>.
- [13] A. Fadaei, A. Salimi, M. Mirzataheri, Structural elucidation of morphology and performance of the PVDF/PEG membrane, *J. Polym. Res.* 21 (2014) 545, <https://doi.org/10.1007/s10965-014-0545-x>.
- [14] B. Imtiaz, N.A. Shepelin, P.C. Sherrell, S.E. Kentish, A.V. Ellis, Direct ink writing of dehydrofluorinated Poly(Vinylidene Difluoride) for microfiltration membrane fabrication, *J. Membr. Sci.* 632 (2021), 119347, <https://doi.org/10.1016/j.memsci.2021.119347>.
- [15] Y. Huang, C. Shang, L. Li, Novel N-doped graphene enhanced ultrafiltration nano-porous polyvinylidene fluoride membrane with high permeability and stability for water treatment, *Separ. Purif. Technol.* 267 (2021), 118622, <https://doi.org/10.1016/j.seppur.2021.118622>.
- [16] G. Zheng, L. Yao, X. You, Y. Liao, R. Wang, J.J. Huang, Effects of different secondary nano-scaled roughness on the properties of omniphobic membranes for brine treatment using membrane distillation, *J. Membr. Sci.* 620 (2021), 118918, <https://doi.org/10.1016/j.memsci.2020.118918>.
- [17] M.S.S.A. Saraswathi, D. Rana, S. Alwarappan, S. Gowrishankar, P. Vijayakumar, A. Nagendran, Polydopamine layered poly (ether imide) ultrafiltration membranes tailored with silver nanoparticles designed for better permeability, selectivity and antifouling, *J. Ind. Eng. Chem.* 76 (2019) 141–149, <https://doi.org/10.1016/j.jiec.2019.03.014>.
- [18] M.S.S.A. Saraswathi, D. Rana, A. Nagendran, S. Alwarappan, Custom-made PEI/exfoliated-MoS₂ nanocomposite ultrafiltration membranes for separation of bovine serum albumin and humic acid, *Mater. Sci. Eng. C* 83 (2018) 108–114, <https://doi.org/10.1016/j.msec.2017.11.015>.
- [19] E. Pramono, M.A. Zakaria, K.F. Fridiasari, S.T.C.L. Ndruru, M. Bagaskara, R.E. Mustofa, et al., Cellulose derived from oil palm empty fruit bunches as filler on polyvinylidene fluoride based membrane for water containing humic acid treatment, *Groundw Sustain. Dev.* 17 (2022), 100744, <https://doi.org/10.1016/j.gsd.2022.100744>.

- [20] S. Liang, K. Xiao, Y. Mo, X. Huang, A novel ZnO nanoparticle blended polyvinylidene fluoride membrane for anti-irreversible fouling, *J. Membr. Sci.* 394–395 (2012) 184–192, <https://doi.org/10.1016/j.memsci.2011.12.040>.
- [21] C. Dong, G. He, H. Li, R. Zhao, Y. Han, Y. Deng, Antifouling enhancement of poly(vinylidene fluoride) microfiltration membrane by adding Mg(OH)₂ nanoparticles, *J. Membr. Sci.* 387–388 (2012) 40–47, <https://doi.org/10.1016/j.memsci.2011.10.007>.
- [22] D. Hou, J. Wang, D. Qu, Z. Luan, X. Ren, Fabrication and characterization of hydrophobic PVDF hollow fiber membranes for desalination through direct contact membrane distillation, *Separ. Purif. Technol.* 69 (2009) 78–86, <https://doi.org/10.1016/j.seppur.2009.06.026>.
- [23] V. Vatanpour, M. Esmaili, S. Shahvari, M. Masteri-Farahani, Evaluation of morphology, performance and fouling tendency of mixed matrix PVDF ultrafiltration membranes incorporated by different size-controlled SAPO-34 nanozeolites, *J. Environ. Chem. Eng.* 9 (2021), 105900, <https://doi.org/10.1016/j.jece.2021.105900>.
- [24] M.S.S.A. Saraswathi, D. Rana, P. Vijayakumar, S. Alwarappan, A. Nagendran, Tailored PVDF Nanocomposite Membranes Using Exfoliated MoS₂ Nanosheets for Improved Permeation and Antifouling Performance, vol. 41, 2017, <https://doi.org/10.1039/c7nj03193a>.
- [25] S.A.M.S. Saraswathi, D. Rana, K. Divya, S. Alwarappan, A. Nagendran, Fabrication of anti-fouling PVDF nanocomposite membranes using manganese dioxide nanospheres with tailored morphology, hydrophilicity and permeation, *New J. Chem.* 42 (2018) 15803–15810, <https://doi.org/10.1039/C8NJ02701C>.
- [26] X. Zhao, C. He, Efficient preparation of super antifouling PVDF ultrafiltration membrane with one step fabricated zwitterionic surface, *ACS Appl. Mater. Interfaces* 7 (2015) 17947–17953, <https://doi.org/10.1021/acsami.5b04648>.
- [27] M. Rao Kotte, T. Hwang, J.-I. Han, M.S. Diallo, A one-pot method for the preparation of mixed matrix polyvinylidene fluoride membranes with in situ synthesized and PEGylated polyethyleneimine particles, *J. Membr. Sci.* 474 (2015) 277–287, <https://doi.org/10.1016/j.memsci.2014.09.044>.
- [28] S.Y. Park, S.H. Choi, J.W. Chung, S.-Y. Kwak, Anti-scaling ultrafiltration/microfiltration (UF/MF) polyvinylidene fluoride (PVDF) membranes with positive surface charges for Ca²⁺/silica-rich wastewater treatment, *J. Membr. Sci.* 480 (2015) 122–128, <https://doi.org/10.1016/j.memsci.2015.01.041>.
- [29] L. Yan, Y.S. Li, C.B. Xiang, S. Xianda, Effect of nano-sized Al₂O₃-particle addition on PVDF ultrafiltration membrane performance, *J. Membr. Sci.* 276 (2006) 162–167, <https://doi.org/10.1016/j.memsci.2005.09.044>.
- [30] M. Baghbanzadeh, D. Rana, T. Matsuura, C.Q. Lan, Effects of hydrophilic CuO nanoparticles on properties and performance of PVDF VMD membranes, *Desalination* 369 (2015) 75–84, <https://doi.org/10.1016/j.desal.2015.04.032>.
- [31] A. Alpatova, M. Meshref, K.N. McPhedran, M. Gamal El-Din, Composite polyvinylidene fluoride (PVDF) membrane impregnated with Fe₂O₃ nanoparticles and multiwalled carbon nanotubes for catalytic degradation of organic contaminants, *J. Membr. Sci.* 490 (2015) 227–235, <https://doi.org/10.1016/j.memsci.2015.05.001>.
- [32] Y. Wei, H.Q. Chu, B.Z. Dong, X. Li, S.J. Xia, Z.M. Qiang, Effect of TiO₂ nanowire addition on PVDF ultrafiltration membrane performance, *Desalination* 272 (2011) 90–97, <https://doi.org/10.1016/j.desal.2011.01.013>.
- [33] Y. Zhang, P. Liu, Preparation of porous ZrO₂ solid superacid shell/void/TiO₂ core particles and effect of doping them on PVDF membranes properties, *Chem. Eng. Sci.* 135 (2015) 67–75, <https://doi.org/10.1016/j.ces.2015.06.037>.
- [34] A. Bottino, G. Capannelli, A. Comite, Preparation and characterization of novel porous PVDF-ZrO₂ composite membranes, *Desalination* 146 (2002) 35–40, [https://doi.org/10.1016/S0011-9164\(02\)00469-1](https://doi.org/10.1016/S0011-9164(02)00469-1).
- [35] R. Koswojo, R.P. Utomo, Y.H. Ju, A. Ayucitra, F.E. Soetaredjo, J. Sunarso, et al., Acid Green 25 removal from wastewater by organo-bentonite from Pacitan, *Appl. Clay Sci.* 48 (2010) 81–86, <https://doi.org/10.1016/j.clay.2009.11.023>.
- [36] F.E. Soetaredjo, L. Laysandra, J.N. Putro, S.P. Santoso, A.E. Angkawijaya, M. Yuliana, et al., Ecological-safe and low-cost activated-bleaching earth: preparation, characteristics, bleaching performance, and scale-up production, *J. Clean. Prod.* 279 (2021), 123793, <https://doi.org/10.1016/j.jclepro.2020.123793>.
- [37] V. Causin, M.L. Carraro, C. Marega, R. Saini, S. Camestrini, A. Marigo, Structure and morphology of solution blended poly(vinylidene fluoride)/montmorillonite nanocomposites, *J. Appl. Polym. Sci.* 109 (2008) 2354–2361, <https://doi.org/10.1002/app.28308>.
- [38] Y.Y. Zhang, S.L. Jiang, Y. Yu, G. Xiong, Q.F. Zhang, G.Z. Guang, Phase transformation mechanisms and piezoelectric properties of poly(vinylidene fluoride)/montmorillonite composite, *J. Appl. Polym. Sci.* 123 (2012) 2595–2600, <https://doi.org/10.1002/app.34431>.
- [39] P. Wang, J. Ma, Z. Wang, F. Shi, Q. Liu, Enhanced separation performance of PVDF/PVP-g-MMT nanocomposite ultrafiltration membrane based on the NVP-grafted polymerization modification of montmorillonite (MMT), *Langmuir* 28 (2012) 4776–4786, <https://doi.org/10.1021/la203494z>.
- [40] C.Y. Lai, A. Groth, S. Gray, M. Duke, Preparation and characterization of poly(vinylidene fluoride)/nanoclay nanocomposite flat sheet membranes for abrasion resistance, *Water Res.* 57 (2014) 56–66, <https://doi.org/10.1016/j.watres.2014.03.005>.
- [41] F. Piscitelli, P. Posocco, R. Toth, M. Fermeglia, S. Pricl, G. Mensitieri, et al., Sodium montmorillonite silylation: unexpected effect of the aminosilane chain length, *J. Colloid Interface Sci.* 351 (2010) 108–115, <https://doi.org/10.1016/j.jcis.2010.07.059>.
- [42] P.T. Bertuoli, D. Piazza, L.C. Scienza, A.J. Zattera, Preparation and characterization of montmorillonite modified with 3-aminopropyltriethoxysilane, *Appl. Clay Sci.* 87 (2014) 46–51, <https://doi.org/10.1016/j.clay.2013.11.020>.
- [43] F. Garcia-Escobar, J. Bonilla-Rios, A.B. Espinoza-Martinez, P. Cerda-Hurtado, Halloysite silanization in polyethylene terephthalate composites for bottling and packaging applications, *J. Mater. Sci.* 56 (2021) 16376–16386, <https://doi.org/10.1007/s10853-021-06337-8>.
- [44] A.M. Abu El-Soad, A.V. Pestov, D.P. Tambasova, V.A. Osipova, N.A. Martemyanov, G. Cavallaro, et al., Insights into grafting of (3-Mercaptopropyl) trimethoxy silane on halloysite nanotubes surface, *J. Organomet. Chem.* 915 (2020), 121224, <https://doi.org/10.1016/j.jorganchem.2020.121224>.
- [45] a M. Shanmugharaj, K.Y. Rhee, S.H. Ryu, Influence of dispersing medium on grafting of aminopropyltriethoxysilane in swelling clay materials, *J. Colloid Interface Sci.* 298 (2006) 854–859, <https://doi.org/10.1016/j.jcis.2005.12.049>.
- [46] E. Pramono, R. Alfiansyah, M. Ahdia, D. Wahyuningrum, C.L. Radiman, Hydrophilic poly(vinylidene fluoride)/bentonite hybrid membranes for microfiltration of dyes, *Mater. Res. Express* 6 (2019), 105376, <https://doi.org/10.1088/2053-1591/ab42e9>.
- [47] T. Sultana, G.L. Georgiev, G. Auner, G. Newaz, H.J. Herfurth, R. Patwa, XPS analysis of laser transmission micro-joint between poly (vinylidene fluoride) and titanium, *Appl. Surf. Sci.* 255 (2008) 2569–2573, <https://doi.org/10.1016/j.apsusc.2008.07.149>.
- [48] S.-H. Yoon, *Membrane Bioreactor Processes: Principles and Applications*, CRC Press: Taylor & Francis Groups, Boca Raton, 2016.
- [49] E.K. Golz, D.A. Vander Griend, Modeling methylene blue aggregation in acidic solution to the limits of factor analysis, *Anal. Chem.* 85 (2013) 1240–1246, <https://doi.org/10.1021/ac303271m>.
- [50] P. Daraei, S.S. Madaeni, E. Salehi, N. Ghaemi, H.S. Ghari, M.A. Khadivi, et al., Novel thin film composite membrane fabricated by mixed matrix nanoclay/chitosan on PVDF microfiltration support: preparation, characterization and performance in dye removal, *J. Membr. Sci.* 436 (2013) 97–108, <https://doi.org/10.1016/j.memsci.2013.02.031>.
- [51] X. Liu, Y. Chen, Z. Deng, Y. Yang, High-performance nanofiltration membrane for dyes removal: blending Fe₃O₄-HNTs nanocomposites into poly(vinylidene fluoride) matrix, *J. Dispersion Sci. Technol.* 42 (2020) 93–102, <https://doi.org/10.1080/01932691.2019.1662308>.
- [52] N. Nikooe, E. Saljoughi, Preparation and characterization of novel PVDF nanofiltration membranes with hydrophilic property for filtration of dye aqueous solution, *Appl. Surf. Sci.* 413 (2017) 41–49, <https://doi.org/10.1016/j.apsusc.2017.04.029>.
- [53] J. Zhao, H. Liu, P. Xue, S. Tian, S. Sun, X. Lv, Highly-efficient PVDF adsorptive membrane filtration based on chitosan@CNTs-COOH simultaneous removal of anionic and cationic dyes, *Carbohydr. Polym.* 274 (2021), 118664, <https://doi.org/10.1016/J.CARBPOL.2021.118664>.
- [54] S. Gholami, J.L. Llacuna, V. Vatanpour, A. Dehqan, S. Paziresh, J.L. Cortina, Impact of a new functionalization of multiwalled carbon nanotubes on antifouling and permeability of PVDF nanocomposite membranes for dye wastewater treatment, *Chemosphere* 294 (2022), 133699, <https://doi.org/10.1016/J.CHEMOSPHERE.2022.133699>.
- [55] Y. Zhao, W. Yu, R. Li, Y. Xu, Y. Liu, T. Sun, L. Shen, H. Lin, Electric field endowing the conductive polyvinylidene fluoride (PVDF)-graphene oxide (GO) nickel (Ni) membrane with high-efficient performance for dye wastewater treatment, *Appl. Surf. Sci.* 483 (2019) 1006–1016, <https://doi.org/10.1016/J.APSUSC.2019.04.054>.
- [56] S. Jahankhah, M.M. Sabzehmeidani, M. Ghaedi, K. Dashtian, H. Abbasi-Asl, Hydrophilic magnetic molecularly imprinted resin in PVDF membrane for efficient selective removal of dye, *J. Environ. Manag.* 300 (2021), 113707, <https://doi.org/10.1016/J.JENVMAN.2021.113707>.